



# Effect of Anodization Treatment on the Thickness, Hardness, and Microstructural Characterization of Anodic Aluminum Oxide Film on AA 6061 and Critical Patent Analysis

Chun-Chieh Lee, Chih-Wei Chen, Jin-Shyong Lin, Shing Hoa Wang, Chiang-Sheng Lee, Chien-Chon Chen, Ya-Hui Lin, and Chih-Yuan Chen

Submitted: 18 October 2020 / Revised: 16 June 2021 / Accepted: 12 August 2021 / Published online: 8 September 2021

The influences of different pre-treatment approaches, comprising sandblasting, grinding, chemical polishing, and plowing, and various anodizing parameters, including electrolyte composition, temperature, current density, time, and final voltage, on the quality of anodized aluminum oxide (AAO) film on AA 6061 were studied in the present research. It was found that, during both mild and hard anodization treatment, the thickness and microhardness of AAO film increased as the anodization current density increased. Under mild anodization treatment, when the current density increased from 0.5 to 2.0 A/dm<sup>2</sup>, the anodization efficiency decreased from 90 to 52% and 71 to 44% during the mild anodization treatment performed at 22°C and 0°C, respectively. However, on the other hand, the anodization efficiency increased from 55 to 56% and 57 to 64% when the current density increased from 7.0 to 8.0 A/dm<sup>2</sup> during the hard anodization treatment carried out at 22°C and 0°C, respectively. Therefore, different AAO film formation mechanisms prevail during the mild and hard anodization treatment. Moreover, the microhardness of AAO film formed at 22°C or 0°C dropped heavily when the current density was higher than 9.0 A/dm<sup>2</sup> due to the burning reaction. In addition, the AAO film can achieve higher hardness and resistance to corrosion through the sealing process, which can effectively decrease the size of the tubes due to the volume expansion effect (23%) after the sealing treatment.

**Keywords** AA 6061, anodization, efficiency, hardness, oxide, pre-treatment

## 1. Introduction

In recent years, the market demand for aluminum alloys to be used in building materials, mechanical components, electrical apparatus, and sports equipment has increased year by year. Light alloys, such as magnesium, aluminum, and titanium-based materials, are low in

density but have a high strength-to-weight ratio, so they are very suitable for engineering materials (Ref 1, 2). The strength-to-weight ratio of aluminum alloys can reach twice that of structural steel, which means the weight of aluminum alloy can be half that of steel for the same strength. Furthermore, unlike other 1xxx to 7xxx aluminum alloys, the 6061 AA is a Al-Mg-Si series heat-treatable strengthened aluminum alloy with an ornamental appearance, namely a glossy, semi-glossy or satin-like glossy exterior, higher specific strength, and good corrosion resistance, so it has become the most widely used aluminum alloy (Ref 2, 3). However, aluminum alloys are soft and prone to corrosion, both of which are characteristics that limit their engineering applications (Ref 3-5).

Surface treatment is a practical solution for materials with a high strength-to-weight ratio but susceptibility to surface degradation. Aluminum alloy is an active material whose surface is very suitable for anodization but not for electro-deposition. Anodic oxide film, which is self-assembled and grows from its parent substrate, gives the surface of aluminum alloy high hardness and very good protection properties. There are many potential applications for anodization. For example, oxide film produced on aluminum by anodization is used for corrosion resistance, wear resistance, electrical resistance, and decoration (Ref 6-10).

The original form of the film is an aluminum oxide layer of the barrier type. In the acid condition, however, the film has a porous-type film structure. During anodization, the applied electric field accelerates hydroxide ions to arrive at the aluminum surface, penetrate the existing oxide film, and combine with the metal aluminum to form a new oxide film. That is, the formation and dissolution of the aluminum oxide film occur in equilibrium with each other to form a porous film with a honeycomb pattern.

The thickness of the natural oxide layer on aluminum pieces is about 5 μm (Ref 9, 10). However, this native oxide film has

Chun-Chieh Lee and Chih-Wei Chen have contributed equally as co-first authors.

**Chun-Chieh Lee**, College of Engineering and Science, Ph.D. Program in Materials and Chemical Engineering, National United University, Miaoli City, Taiwan; **Chih-Wei Chen**, Division of Neurosurgery, Department of Surgery, Chi Mei Medical Center, Tainan 710, Taiwan; and Department of Occupational Safety and Health/Institute of Industrial Safety and Disaster Prevention, College of Sustainable Environment, Chia Nan University of Pharmacy and Science, Tainan 717, Taiwan; **Jin-Shyong Lin**, Department of Mechanical Engineering, National Chin-Yi University of Technology, Taichung City, Taiwan; **Shing Hoa Wang**, Department of Mechanical and Mechatronic Engineering, National Taiwan Ocean University, Keelung, Taiwan; **Chiang-Sheng Lee** and **Chien-Chon Chen**, Department of Energy Engineering, National United University, Miaoli City, Taiwan; **Ya-Hui Lin** and **Chih-Yuan Chen**, Graduate Institute of Intellectual Property, National Taipei University of Technology, Taipei, Taiwan. Contact e-mails: ccchen@nuu.edu.tw and chen6563@gmail.com.

high porosity and low mechanical strength, which implies that aluminum alloys without adequate surface treatment have limited corrosion resistance in certain environments, such as industrial environments. On the other hand, an artificial anodic oxide film with a larger and controllable thickness and a porous structure can be obtained by anodizing aluminum metal in acid solution. Moreover, this thicker oxide film has excellent hardness and resistance to corrosion and wear. Due to the high porosity of the anodic oxide film, the film formed on the metal can be further used for electroplating, painting, and decorative coloring (Ref 11-13). In addition, due to its regular arrangement on the surface of aluminum alloy, such anodic oxide film is also widely utilized in the medical field for bio-chip fabrication (Ref 14-16), protein purification engineering (Ref 17-19), DNA sequence identification (Ref 19), cell growth (Ref 20-22), tissue engineering (Ref 21), drug release (Ref 23, 24), and x-ray scintillation screens (Ref 25).

Aluminum anodization can be processed in an acid or alkaline bath (Ref 12). Unlike the oxalic, chromic and phosphoric acid baths, the sulfuric acid bath is the most commonly used in industry. It has the advantages of low cost, rapid action, and comparatively low operating voltage, so it is commonly used in anodization processes (Ref 11).

In general, industrial anodization processes include multiple steps: degreasing, alkaline etching, anodization, electrolysis coloring, electrophoresis, sealing, and air drying. The steps of anodizing used in industrial production can be summarized as follows: (1) moving the aluminum work-piece into a sulfuric acid bath (90 g/L, room temperature, 4 min) for acid cleaning, (2) removing the degreased work-piece for water washing, (3) moving the aluminum work-piece into alkaline solution with sodium hydroxide for alkaline washing (50 g/L, 50°C, 3min), (4) water washing before alkaline etching of the aluminum work-piece, (5) anodization (20°C, 1.2 A/dm<sup>2</sup>), (6) water washing after anodization of the aluminum work-piece, (7) moving the anodized work-piece into a bath comprising tin sulfate 8 g/L and nickel sulfate 17 g/L and electrolyte for coloring (21°C, 200 sec, 21V), (8) moving the colored work-piece into an electrophoresis bath (5 g/L, conductivity 900  $\mu$  s, pH = 8, 120 V), (9) sealing, and (10) curing (50 min, 180°C) (Ref 26-29).

The resulting anodic oxide film is porous and has good permeability, so the surface of aluminum alloy can be soaked with organic or inorganic dyes, which penetrate into the capillary pores to form a variety of colors on the finished products. It is generally used for surface modification and is also known as decorative mild anodization. The thickness resulting from mild anodization is below 10  $\mu$ m (Ref 28). Because of the fierce competition in decorative anodizing, major anodizing manufacturers are also actively developing new markets so that the anodizing process can be smoothly included as a key process in the next generation of products. Once a new target product is developed for anodizing, it is expected to become a slice of the pie that manufacturing industries compete for (Ref 30-33).

Research on the surface characteristics of aluminum alloy and the microstructure of aluminum anodic oxide film has attracted great attention (Ref 34-39). Generally, the growth parameters of anodized aluminum films are easily affected by process conditions, such as the current density, temperature, and electrode distance. The high quality of controllable anodic film is well known in academic research (Ref 6). However, many engineering problems still need to be overcome to

promote its application in industry. For example, the anodic oxide growth rate is a challenging problem because local reaction heat easily induces pitting and burnout on the anodic oxide film, which can lead to failure of the anodization (Ref 11). Therefore, to overcome the local heat or exothermic reaction problem, a new anodization mold and bath system were developed in the present study. The objective of this study was to investigate the formation of anodic oxide film by a sulfuric acid electrolyte anodizing process. Moreover, to develop deep insight on the effects of the various anodization conditions on the quality of the resultant anodized film, such as anodization efficiency, film hardness, film color, and film microstructure, various anodization parameters were used in the present study.

Since anodization processes are sensitive to the operation conditions, defects will appear in anodic film if unsuitable conditions are applied. The controllable conditions include the electrolyte composition, temperature, applied voltage, cooling cycle, and current density. In anodization, the working electrode presents an exothermic reaction. Thus, when preparing small-scale samples for academic research, it is not a problem to deal with the small heat quantity of the exothermic reaction. In mass production, however, the maintenance of a constant current density and temperature are critical issues, especially in the case of large Al workpieces. Therefore, in the present study, we designed the electrochemical mold and the chemical bath, and we controlled the complicated anodization parameters to verify that high-quality anodic aluminum oxide film could be formed on a large Al specimen if the reaction heat could be dissipated efficiently.

## 2. Experimental Procedure

The experimental procedure is shown in Fig. 1. The anodic oxide film was formed on the AA 6061 by anodization in the present study. The experimental procedure can be primarily categorized into three stages: pre-treatment, anodizing, and post-treatment. The main experimental conditions of the aluminum surface pre-treatments, anodization, and post-treatment are described as follows:

### 2.1 Aluminum Surface Pre-Treatments

To release the residual stress from rolling, the 4-inch-diameter disk of AA 6061 was first annealed in an air furnace at 120°C for 1h. Second, the Al disk was mechanically ground to remove any obvious scratches. Then the surfaces were further polished by both chemical polishing (85% H<sub>3</sub>PO<sub>4</sub>, at 95°C for 2 min) and electrolytic polishing (15 vol.% HClO<sub>4</sub> + 15 vol.% (CH<sub>3</sub>(CH<sub>2</sub>)<sub>3</sub>OCH<sub>2</sub>CH<sub>2</sub>OH + 70 vol.% C<sub>2</sub>H<sub>6</sub>O, at 25 V and 0°C for 15 min).

### 2.2 Anodizing

The anodization included mild anodization (10 vol.% H<sub>2</sub>SO<sub>4</sub>, at 20 min and 0°C, and 22°C) for anodic oxide film with low hardness, and hard anodization (5 vol.% H<sub>2</sub>SO<sub>4</sub> + 6 vol.% C<sub>2</sub>H<sub>6</sub>O<sub>2</sub> + 2.4 wt.% C<sub>2</sub>H<sub>2</sub>O<sub>4</sub>, at -4°C) for anodic oxide film with high hardness.

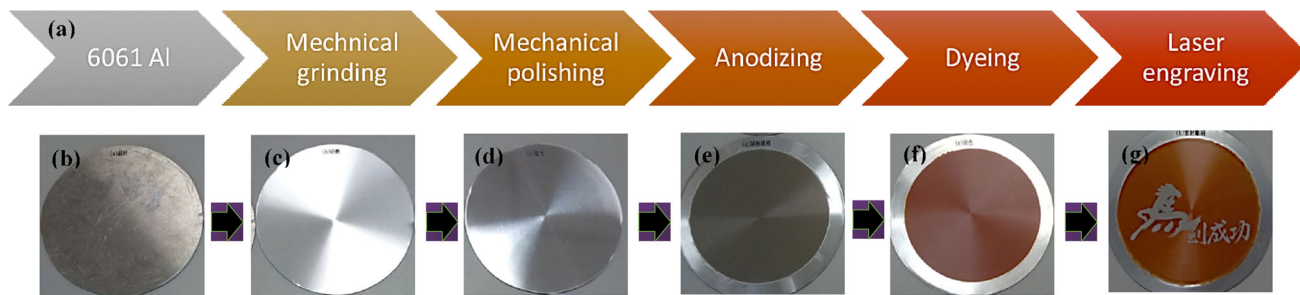


**Fig. 1** (a) Flow chart illustrating the entire experiment process. (b-g) Steps of anodizing and patterning on AA 6061 surface; (b) 4-inch AA 6061 disk, (c) mechanical grinding, (d) mechanical polishing, (e) anodizing, (f) dyeing, (g) electrophoresis

### 2.3 Anodic Film Post-Treatments

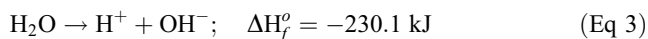
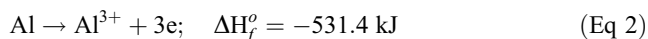
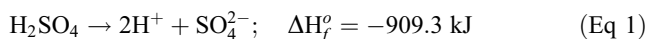
For decoration, identification, and patterning purposes, the anodic oxide film was dyed (commercial dye, 5g/L, 40°C, 5 min) with varied colors. The colors were stabilized by sealing (H<sub>2</sub>O, 100°C, 40 min), a high-quality surface was ensured by polishing, patterning was accomplished by engraving, and partial surface protection was conferred by electrophoresis (commercial electrophoretic paint, 6g/L solution, 50°C, 2 min).

The microstructures of the AA 6061 and anodic oxide film were characterized by optical microscopy (OM, Nikon LV 150), scanning electron microscopy (SEM, 10 kV, HITACHI Regulus 8100 Field emission scanning electron microscopy (FE-SEM)), and transmission electron microscopy (TEM, JEOL-2100F, 200 kV). The free-standing anodic oxide film for TEM observation was made by removing the aluminum substrate with an aqueous etching solution (8 vol.% HCl + saturation CuCl<sub>2</sub>, 25°C, 20 min). Moreover, the chemical compositions of the AA 6061 and anodic oxide films were measured using energy dispersive X-ray spectroscopy (EDS) and element mapping. The hardness data were obtained by a Vickers hardness tester (FM-300e, Future-Tech Corp.) with a load of 1000 g and averaged from measurements at 20 different sites near the joint regions. In addition, the electrochemical behavior was examined by AC impedance measurement and Tafel polarization test (Zahner Impedance Measuring Unit (IM 6)).

## 3. Results and Discussions

Figure 2 shows the anodization mold and anodization bath system used in the present study. The present anodization process has the following three main features: (1) The anodization mold with the anodization reaction area (4 inches in diameter) is made of Teflon and uses copper as a conductor; (2) the exploded view includes an up-cover with an anodization reaction area, a silicone ring as the water sealing material, a copper plate and rod as conductivity conductors, and an aluminum sheet set between the silicone ring and copper plate; and (3) the anodization bath system includes a cooler, pump, filter, heat exchange plate, and anodization bath.

Because the anodization reaction produces heat when metals or components are ionized in the anodization processes, the ionization reactions include Eq 1-3, which are all exothermic reactions (1), where  $\Delta H$  is standard enthalpy.



This large amount of exothermic reaction heat affects the anodization temperature and makes the electrochemical reaction less stable (Ref 9, 13). To maintain a stable anodization temperature in the reaction, we designed an anodization bath system, shown in Fig. 2(c). The main feature of the anodization bath is that it can keep the temperature stable during the entire anodization process due to the cycling by a pump of the electrolyte between the anodization bath and the cooler bath with a heat exchange plate.

Figure 3(a) and (b) shows OM and SEM images of the original AA 6061, which present many obvious rolling traces regularly dispersed within the Al alloy. Moreover, the main elements, Al, Mg, and Si, can be also found in the EDS spectrum (Fig. 3c). After the electro-polishing treatment, the parent AA 6061 revealed obvious white light  $\alpha$ -Al phase along with some particles randomly precipitated within the  $\alpha$ -Al grains (Fig. 3d). According to previous studies (Ref 40-42), these precipitates, Mg<sub>2</sub>Si, contribute strength to the Al alloy. Furthermore, the Al alloy had a clear surface without any scratches after the electro-polishing treatment, which was critical for the following anodization treatment (Fig. 3d).

To obtain surfaces of different roughness on the AA 6061, the surfaces were pretreated. Retained stress was released by annealing, and scratches were removed by sandpaper grinding. Then a uniform surface roughness was created by sandblasting, plowing, mechanical polishing, and chemical polishing. Fig. 4 shows OM and atomic force microscopy (AFM) images of the surface of the AA 6061 after sandpaper grinding, sandblasting, plowing, and chemical polishing. The following information was obtained from observations of the microscopic images: (1) The AA 6061 surface still retained straight sandpaper traces after grinding; (2) the surface was uniformly roughened after sandblasting (# 80, Al<sub>2</sub>O<sub>3</sub> powder); (3) a surface with holes presented after plowing, and (4) the surface presented a porous film ( $\text{Al} + \text{H}_3\text{PO}_4 \rightarrow \text{Al}(\text{H}_2\text{PO}_4) + \text{H}_2$ ) after chemical polishing. Table 1 shows the surface roughness of AA 6061 after sandblasting, chemical polishing, grinding, plowing, mild anodization, and hard anodization treatments. The maximum roughness on the aluminum alloy surface ( $R_a = 2.38 \mu\text{m}$ ) was obtained after sandblasting (# 80), and the minimum roughness of  $R_a = 0.27 \mu\text{m}$  presented after grinding and plowing. The surface roughness treatments of grinding, blasting, plowing, and polishing could be used to control the surface roughness of

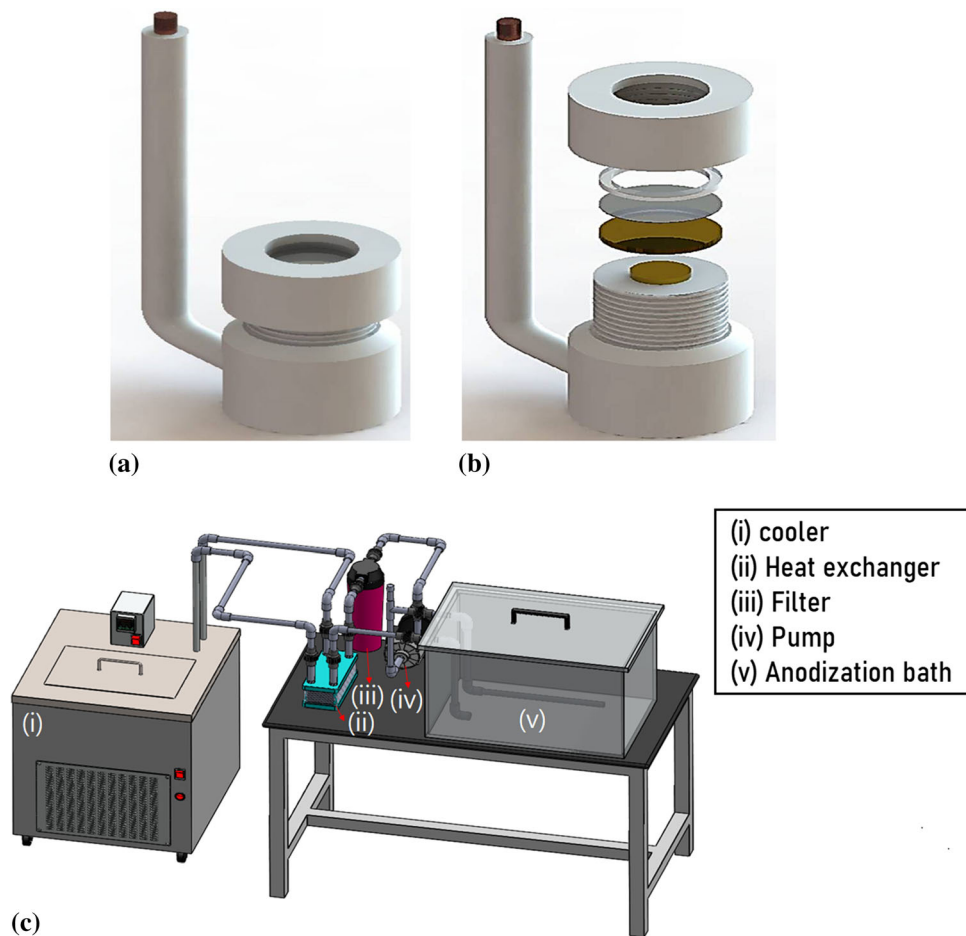


**Fig. 2** Schematic diagrams showing experimental facility setup. (a) anodizing mold, (b) exploded view of anodizing mold, and (c) anodization bath

$R_a$  to between 0.27 and 2.38  $\mu\text{m}$ . Therefore, AA 6061 can present a smooth shiny surface with a surface roughness of  $R_a$  0.31  $\mu\text{m}$  or an anti-reflection surface with a surface roughness of  $R_a$  1.83  $\mu\text{m}$ .

It is generally accepted that  $\text{Al}^{3+}$  ions can form from aluminum alloy in an acid aqueous solution at a specific voltage. Therefore, based on the reaction formula, the relationship of ion concentration and equilibrium potential can be drawn into a graph; i.e., a Pourbaix diagram (Ref 39). In the Al Pourbaix diagram, when the electrolyte pH value is kept below 4 and the applied voltage is higher than  $-1.8\text{V}$  (Ref SHE), anodic aluminum oxide (AAO) can form on the surface of Al alloy. The structure of AAO is a honeycomb-like tubular structure, and each cell has a circular hole in the middle. During the anodization, the applied voltage causes the oxide film to continue growing and the film to expand in volume, squeezing the holes against each other. The holes generate repulsive forces between them, and the anodic film expands to form a dense hexagonal stacking structure.

Figure 5 shows the results of Al alloy specimens covered in aluminum oxide films of various colors after undergoing mild anodization treatment ( $50\text{ cm}^2$ ,  $22^\circ\text{C}$ , and 20 min) at different current densities (1-12  $\text{A}/\text{dm}^2$ ). It can be clearly seen that the aluminum oxide film was variably translucent, brown, or black when the current densities were at 1 to 4, 5 to 8, and 9 to 12  $\text{A}/\text{dm}^2$ , respectively. Moreover, these oxide films of different

colors are suitable for distinct purposes. For example, only translucent aluminum oxide film is suitable for dyeing to any kind of color (Ref 9, 10). However, aluminum oxide film that is brown or black in color is not suitable for dyeing due to its deep color. Ref 21, 28. On the other hand, Fig. 6 shows the results of Al alloy specimens covered in aluminum oxide films of various colors after undergoing mild anodization treatment ( $50\text{ cm}^2$ ,  $0^\circ\text{C}$ , and 20 min) at different current densities (1-12  $\text{A}/\text{dm}^2$ ). It can be clearly seen that the aluminum oxide film was variably translucent, brown, or black, or had partial burring, when the current densities were fixed at 1 to 4, 5 to 6, 7 to 9, and 10 to 12  $\text{A}/\text{dm}^2$ , respectively. To understand the influence of the anodizing temperature on the quality of the aluminum oxide film, some detailed experimental results of anodizing treatments at 0 and  $22^\circ\text{C}$  are presented in Tables 2 and 3, respectively.

The anodic aluminum oxide reaction can be expressed as  $\text{Al}^{3+} + 3\text{OH}^- \rightarrow \text{Al}(\text{OH})_3$  (Ref 1, 41, 42). According to Faraday's laws, the relationship between anodic current and film thickness can be expressed as Eq 4, which can be further simplified to Eq 5:

$$Q = It = nFN = nF\rho DA/M \quad (\text{Eq 4})$$

$$D = ItM/nF\rho A \quad (\text{Eq 5})$$

where  $Q$  is power (C),  $I$  is current (A),  $T$  is time (sec),  $n$  is valence,  $F$  is Faraday constant (i.e., 96,500),  $N$  is mole,  $\rho$  is

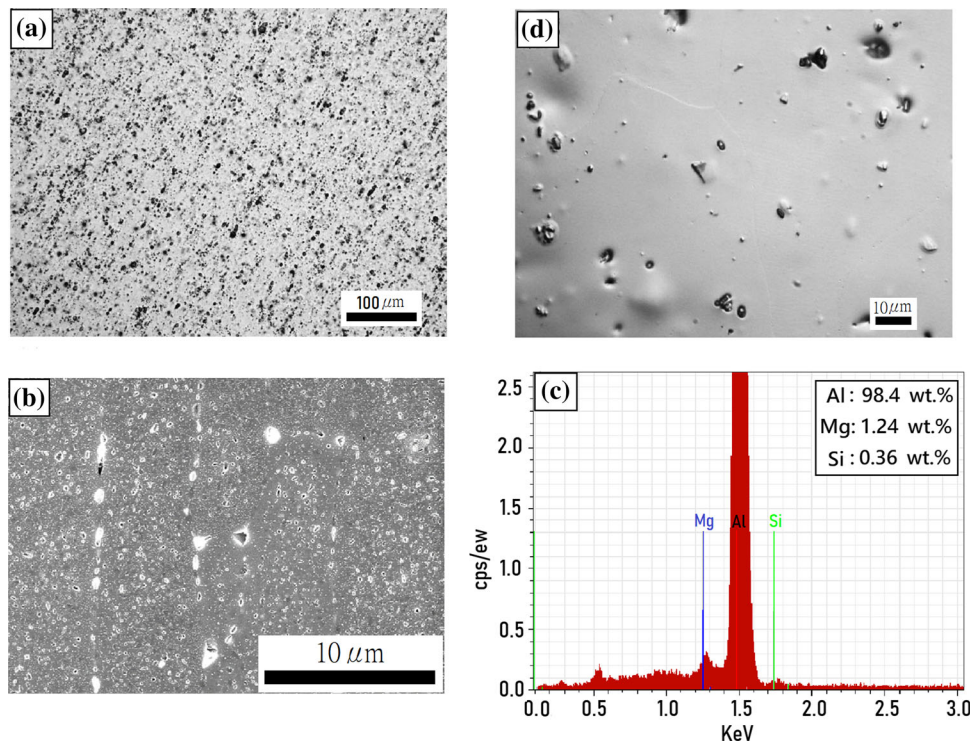


**Fig. 3** Surface morphologies (a, d) Optical microscopy morphologies, (b) SEM image, and (c) corresponding EDS analysis of original AA 6061 before (a, b) and after (d) electro-polishing treatment

density ( $\text{g}/\text{cm}^3$ ),  $D$  is thickness (cm),  $A$  is surface area ( $\text{cm}^2$ ), and  $M$  is molecular weight ( $\text{g}/\text{mol}$ ).

In the present study, the anodizing time was 1200 seconds, and the anodizing area was  $50 \text{ cm}^2$ . Therefore, Eq 5 can be simplified to Eq 6, and the anodization efficiency can be calculated using Eq 7, where  $D_a$  and  $D$  are experimental thickness and calculation thickness, respectively.

$$D(\mu\text{m}) = 26.94 \times I \quad (\text{Eq } 6)$$

$$\eta(\%) = 100 \times D_a/D \quad (\text{Eq } 7)$$

In Table 2, the anodization treatment at  $22^\circ\text{C}$  can be divided into four regions: mild anodization, with a current density of  $0.5\text{-}2 \text{ A}/\text{dm}^2$  (region I); semi-hard anodization, with a current density of  $3.0\text{-}6.0 \text{ A}/\text{dm}^2$  (region II); hard anodization, with a current density of  $7.0\text{-}8.0 \text{ A}/\text{dm}^2$  (region III); and burring, with a current density higher than  $9.0 \text{ A}/\text{dm}^2$  (region IV). The mild anodization presented after a lower final voltage of  $7\text{-}17 \text{ V}$  and produced a hardness of  $142\text{-}185 \text{ HV}_{1.0}$ . In contrast, the hard anodization presented after a higher final voltage of  $30\text{-}43 \text{ V}$  and produced a hardness of  $335\text{-}359 \text{ HV}_{1.0}$ . The burring anodization presented after an unstable final voltage, thickness, and efficiency, and the hardness was  $329\text{-}168 \text{ HV}_{1.0}$ . The anodization efficiency had a high value of  $90\%$  at the lower current density of  $0.56 \text{ A}/\text{dm}^2$ . The efficiency was lower ( $52\text{-}56\%$ ) when the current density was higher than  $2 \text{ A}/\text{dm}^2$ . Similar results were obtained with the anodization treatment at  $0^\circ\text{C}$ , as can be seen in Table 3. From comparing Table 2 with 3, it was deduced that when the anodizing treatment occurs at a lower temperature, then a long anodization time, higher anodization voltage, and higher current density are needed

due to the anodized oxide film tending to form slowly in the electrolyte. The reason is that two primary mechanisms, the growth mode and the dissolving mode, compete with each other during the anodizing treatment (Ref 8, 12, 15). Furthermore, the growth mechanism dominates at low anodizing temperature, resulting in a thicker alumina oxide film after anodizing treatment. On the other hand, the thickness of anodized oxide film increases slowly at high temperature because the dissolving mechanism prevails.

Figure 7 shows samples of AA 6061 after mild anodization at different temperatures under the same reaction area ( $50 \text{ cm}^2$ ) and time (20 min). Several valuable points can be deduced from Fig. 7, as follows: (1) The final voltage value can be used to evaluate the anodic oxide film thickness and resistance properties because a higher final voltage leads to higher film thickness and resistance; (2) the theoretical anodization oxide film thickness can be calculated by Eq 6. Moreover, the oxide film thickness is proportional to the current density; (3) The anodization efficiency can be calculated by Eq 7. Comparing the anodization temperatures of  $22$  and  $0^\circ\text{C}$ , the anodic oxide films had lower anodization efficiency; (4) Anodic oxide film with a higher hardness can be obtained at a lower anodization temperature ( $0^\circ\text{C}$ ).

Figure 8 shows the partial burring region within the anodic oxide film, which was caused by a high anodization current density. It was also found that the burring zone began at the mold edge when the current density reached  $10.0 \text{ A}/\text{dm}^2$  (Fig. 8a). Holes were burned in the anodic oxide films when the current density rose to  $12.0 \text{ A}/\text{dm}^2$  (Fig. 8b). Furthermore, the burring zone had a lower hardness than did the other normal anodized film regions. For example, the hardness values at

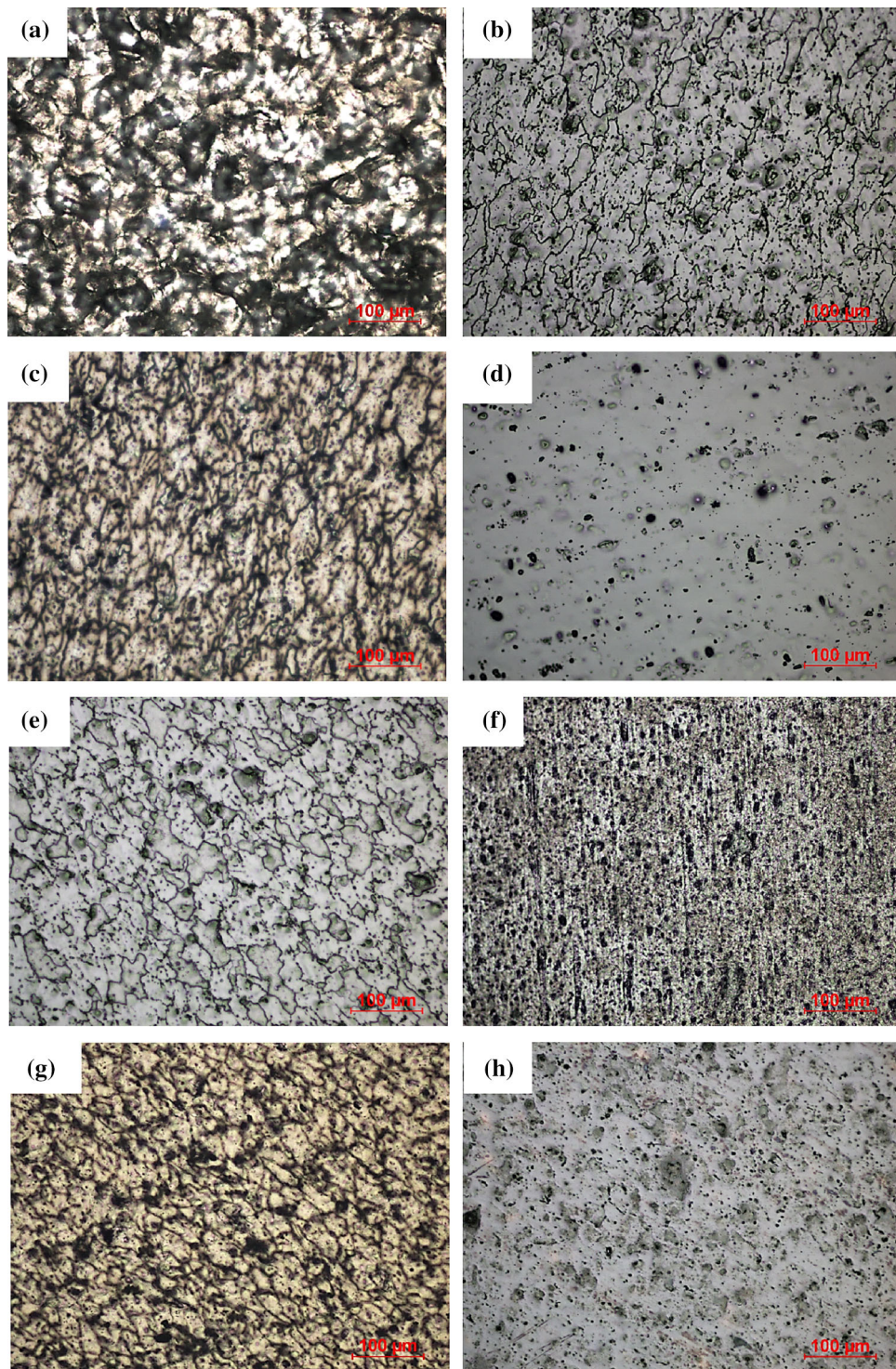


**Fig. 4** (a-h) Optical microscopy morphologies and (i-p) AFM images of 6061 aluminum alloy after different surface pre-treatments: (a, i) sandblasting, (b, j) sandblasting and chemical polishing, (c, k) sandblasting, chemical polishing and mild anodizing, (d, l) grinding, (e, m) grinding and chemical polishing, (f, n) grinding and plowing, (g, o) grinding, plowing and mild anodizing, and (h, p) grinding, plowing, and hard anodizing

points 1, 2, 3, and 4 were 468, 450, 320, and 293  $HV_{1.0}$ , respectively, when the anodization treatments were performed at  $10.0 \text{ A/dm}^2$  (Fig. 8a). Similarly, the hardness values at points 1, 2, 3, and 4 were 402, 320, 105, and 50  $HV_{1.0}$  when the anodization treatment was performed at  $12.0 \text{ A/dm}^2$  (Fig. 8b).

From Table 2 and 3 and Fig. 8, it was deduced that a good quality of mild anodized film can be achieved at a current density below  $2.0 \text{ A/dm}^2$ . On the other hand, when the current density is higher than 9.0 or the final voltage is higher than 50 V, the anodization oxide film tends to be burned out (unsuitable anodization).

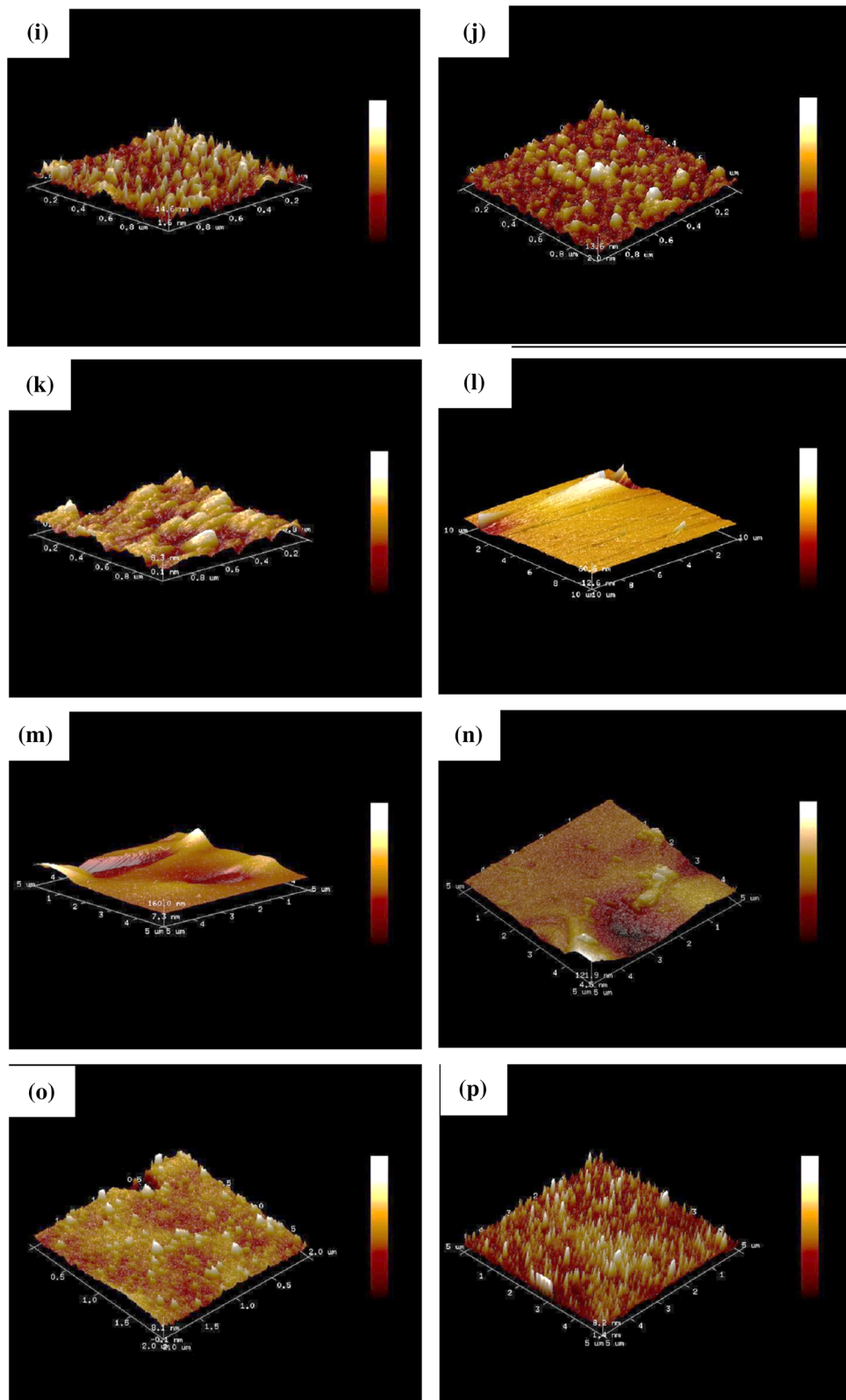


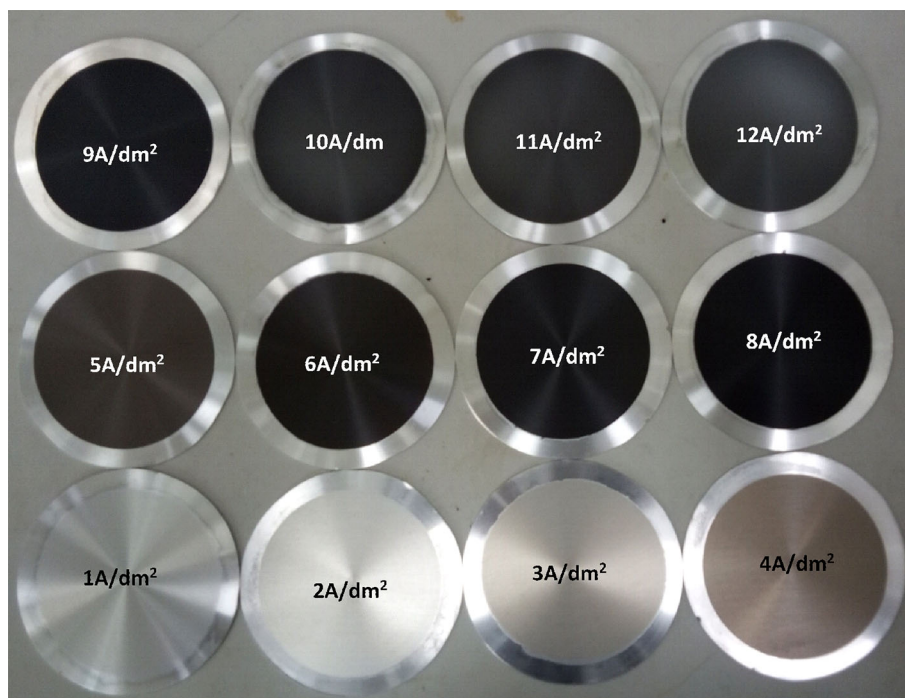
Fig. 4 continued

To further increase the film hardness and anodization efficiency, the hard anodization conditions were modified in the present research. For example, the hard anodization

temperature was lowered to  $-4^{\circ}\text{C}$  instead of being kept at  $22^{\circ}\text{C}$  or  $0^{\circ}\text{C}$ . The chemical composition of the hard anodization aqueous electrolyte was modified to 5 vol.%  $\text{H}_2\text{SO}_4$  + 6 vol.%

**Table 1** Surface roughness of AA 6061 after various surface pre-treatments

Surface pre-treatment	Roughness, $R_a$ $\mu\text{m}$
1. Sandblasting	$2.38 \pm 0.3$
2. Sandblasting + Chemical Polishing	$1.64 \pm 0.5$
3. Sandblasting + Chemical Polishing + Mild Anodizing	$1.83 \pm 0.3$
4. Grinding	$0.12 \pm 0.4$
5. Grinding + Chemical Polishing	$0.47 \pm 0.6$
6. Grinding + Plowing	$0.27 \pm 0.2$
7. Grinding + Plowing + Mild Anodizing	$0.31 \pm 0.3$
8. Grinding + Plowing + Hard Anodizing	$0.65 \pm 0.4$

**Fig. 5** Images of films of various colors produced under mild anodization conditions of 1-12 A/dm<sup>2</sup>, 50 cm<sup>2</sup>, 22 °C, and 20 min

C<sub>2</sub>H<sub>6</sub>O<sub>2</sub> + 2.4 wt.% C<sub>2</sub>H<sub>2</sub>O<sub>4</sub>. In addition, a two-step current density approach was utilized in the anodization process, as follows: In the first step, the current density was increased from 0 to 2.0, 3.0, or 4.0 A/dm<sup>2</sup> within 20 min; in the second step, the current density was maintained at 2.0, 3.0, or 4.0 A/dm<sup>2</sup> until the final voltage of 70 V. Fig. 9 shows the I-V and I-T curves of AA 6061 under hard anodization with experimental parameters of 50 cm<sup>2</sup> and -4°C. The quantities of electricity in the two-step current density approach were 4410 C, 4050 C, and 4200 C when the current densities were 2.0, 3.0, 4.0 A/dm<sup>2</sup> in the voltage range of 0-70 V, respectively. As shown in Table 4, the anodic oxide film and anodization efficiency were 576 HV<sub>1.0</sub> and 60% when the current density and final voltage were 2.0 A/dm<sup>2</sup> and 70V.

Figure 10 presents TEM images of anodic oxide films formed on AA 6061. Several microstructural characteristics were observed in these images. The first was an anodic oxide film with a hollow tube structure, which had an outside diameter of 240-280 nm and an inner diameter of 70-90 nm.

Second, the tube surface had a random texture. Third, from EDS analysis and element mapping images, it was found that the tubes mainly consisted of Al (62.31 wt.%), Mg (1.21 wt.%), Si (0.30 wt.%), and O (36.18 wt.%). Fourth, the tubes had an amorphous structure. When aluminum is placed in a specific electrolyte under suitable anodization conditions, the oxide film forms a regular cell or nanotube structure, and the bottom of a nanotube, which is between a barrier layer and the aluminum substrate, forms a hemispherical shape (Ref 9, 10). The characteristics of the barrier layer, diameter of the nanotube, tube density, pore wall thickness, and tube length depend on the anodization parameters.

AA 6061 is a precipitation hardening alloy; the alloying elements Mg and Si precipitate and form Mg<sub>2</sub>Si in the anodic oxide film during anodization (Ref 2-5). The microscopic morphologies showed that the nanotubes had a random texture on the surface. That is the reason why, when the aluminum substrate was removed, the separate anodic film exhibited brittleness.



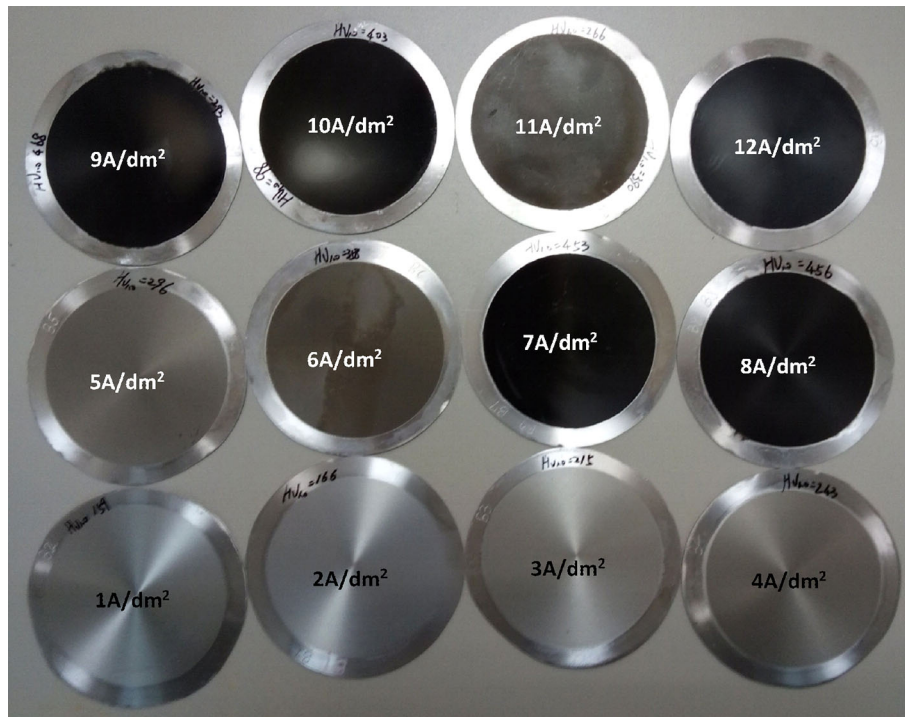


Fig. 6 Images of films of various colors produced under mild anodization conditions of 1-12 A/dm<sup>2</sup>, 50 cm<sup>2</sup>, 0°C, and 20 min

Table 2 Thickness and hardness of anodized aluminum oxide film obtained by anodization treatment of AA 6061 (50 cm<sup>2</sup>) at 22°C for 20 min under different conditions

Symbol	Treatment	Current, A	Current density, A/dm <sup>2</sup>	Power, C	Final voltage, V	Measured thickness, μm	Calculated thickness, μm	Anodization efficiency, %	Hardness, HV <sub>1.0</sub>
H-M1	Mild Anodization	0.28	0.56	336	7	6.8	7.5	90	142 ± 7
H-M2	Mild Anodization	0.4	0.8	300	8	8	11	73	148 ± 10
H-M3	Mild Anodization	0.5	1.0	600	12	10	13	71	163 ± 6
H-M4	Mild Anodization	1.0	2.0	1200	17	14	27	52	185 ± 7
H-S1	Semi-Hard Anodization	1.5	3.0	1800	20	22	40	54	196 ± 4
H-S2	Semi-Hard Anodization	2.0	4.0	2400	22	28	54	52	197 ± 7
H-S3	Semi-Hard Anodization	2.5	5.0	3000	24	36	67	53	255 ± 9
H-S4	Semi-Hard Anodization	3.0	6.0	3600	27	45	81	56	312 ± 7
H-H1	Hard Anodization	3.5	7.0	4200	30	52	94	55	335 ± 15
H-H2	Hard Anodization	4.0	8.0	4800	43	60	108	56	359 ± 11
H-B1	Burring	4.5	9.0	5400	50 → 40	75 ~ 65	121	54~61	329 ± 13
H-B2	Burring	5.0	10.0	6000	50 → 40	88 ~ 75	134	56~65	292 ± 10
H-B3	Burring	5.5	11.0	6600	50 → 40	80 ~ 92	148	53~62	189 ± 6
H-B4	Burring	6.0	12.0	7200	50 → 40	108 ~ 95	161	59~67	168 ± 7

The anodic oxide films formed primarily through deposition (film growth) and dissolution (film dissolving) mechanisms. Thus, the anodized films contained pores and some moisture after anodization. Therefore, for use in industry, a dense anodic

film must be obtained through a sealing procedure. The method of sealing is usually to immerse the anodic film in boiling water for a period of time. After the sealing procedure, the anodic

**Table 3 Thickness and hardness of anodized aluminum oxide film obtained by anodization treatment of AA 6061 (50 cm<sup>2</sup>) at 0 °C for 20 min under various conditions**

Symbol	Treatment	Current, A	Current density, A dm <sup>-2</sup>	Power, C	Final voltage, V	Measured thickness, μm	Calculated thickness, μm	Anodization efficiency, %	Hardness, HV <sub>1.0</sub>
L-M1	Mild Anodization	0.25	0.5	300	24	5	7	71	130 ± 6
L-M2	Mild Anodization	0.5	1.0	600	26	9	13	69	159 ± 7
L-M3	Mild Anodization	1.0	2.0	1200	27	12	27	44	166 ± 5
L-S1	Semi-Hard Anodization	1.5	3.0	1800	29	20	40	50	215 ± 8
L-S2	Semi-Hard Anodization	2.0	4.0	2400	30	27	54	50	243 ± 6
L-S3	Semi-Hard Anodization	2.5	5.0	3000	35	38	67	57	296 ± 10
L-S4	Semi-Hard Anodization	3.0	6.0	3600	45	49	81	60	358 ± 12
L-H1	Hard Anodization	3.5	7.0	4200	52	54	94	57	453 ± 13
L-H2	Hard Anodization	4.0	8.0	4800	63	70	108	64	456 ± 12
L-B1	Burring	4.5	9.0	5400	74 → 71	57 ~ 76	121	47~62	293 ± 6
L-B2	Burring	5.0	10.0	6000	87 → 65	70 ~ 100	134	52~74	98 ± 5
L-B3	Burring	5.5	11.0	6600	110 → 50	85 ~ 95	148	57~64	85 ± 7
L-B4	Burring	6.0	12.0	7200	1000 → 45	70 ~ 100	161	43~62	50 ± 6

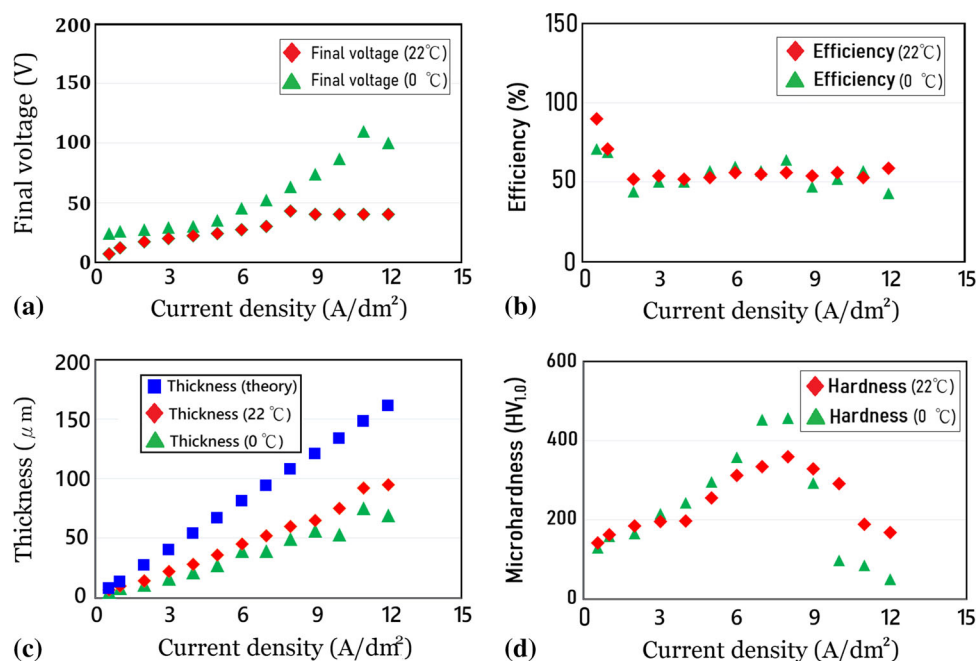


**Fig. 7** The variation of (a) applied power, (b) anodization efficiency, (c) thickness, and (d) hardness with current density for AA 6061 under anodizing treatment conditions at 22 °C and 0 °C

oxide film can achieve the advantages of increased film hardness, anti-pollution, and corrosion resistance (Ref 33).

The sealing process converts amorphous Bayerite, i.e., aluminum trihydrate (Al<sub>2</sub>O<sub>3</sub>·3H<sub>2</sub>O or 2Al(OH)<sub>3</sub>) containing 85% Al<sub>2</sub>O<sub>3</sub>, into Boehmite, i.e., aluminum monohydrate (Al<sub>2</sub>O<sub>3</sub>·H<sub>2</sub>O or 2AlO(OH)), through the hydration reaction of anodic film in pure water at the boiling point. The sealing reaction of anodic film from the conversion of Bayerite into Boehmite can be expressed as Eq 8 (6-10, 33, 43, 44).



Because the molecular volume of Boehmite is larger than that of Bayerite, the volume expansion causes the micro-pores

of the anodic oxide film to be filled and closed. The volume expansion of the above phase transformation can be calculated with Eq 9, where V is volume (cm<sup>3</sup>), M is molecular weight (g/mole), and ρ is density (g/cm<sup>3</sup>). Based on Eq 9, the volumes of 1 mole AlO(OH) (ρ: 3.03 g/cm<sup>3</sup>, M: 60 g/mole), Al(OH)<sub>3</sub> (ρ: 2.53 g/cm<sup>3</sup>, M: 78 g/mole), and H<sub>2</sub>O (ρ: 1.0 g/cm<sup>3</sup>, M: 18 g/mole) can be calculated as 19.8 cm<sup>3</sup>, 30.8 cm<sup>3</sup>, and 18.0 cm<sup>3</sup>. Based on Eq 8, the anodic film volume expands from 30.8 cm<sup>3</sup> to 37.8 cm<sup>3</sup>, an increase of 23%.

$$V = \text{mole} \times M / \rho \quad (\text{Eq 9})$$

Figure 11 presents TEM morphologies of AA 6061 anodic film before and after the sealing treatment. The size of the

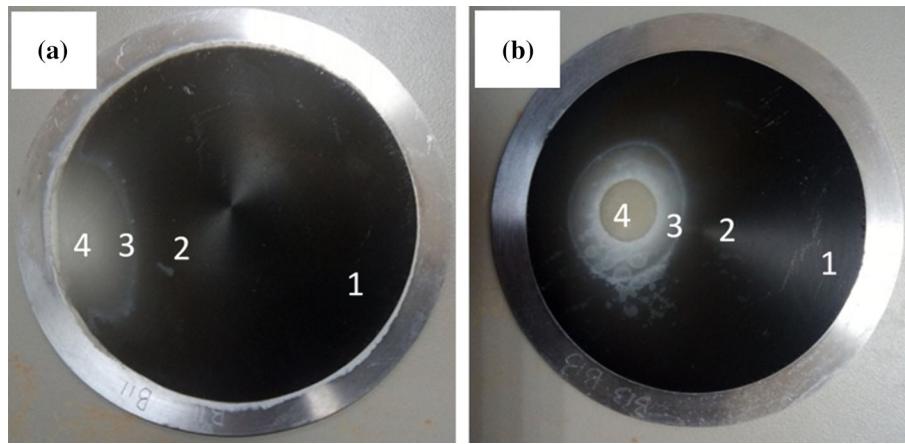


**Fig. 8** The appearance of the partial burring region on the surface of AA 6061 after anodizing treatment at various current densities: (a) 10.0 A/dm<sup>2</sup>, (b) 12.0 A/dm<sup>2</sup>

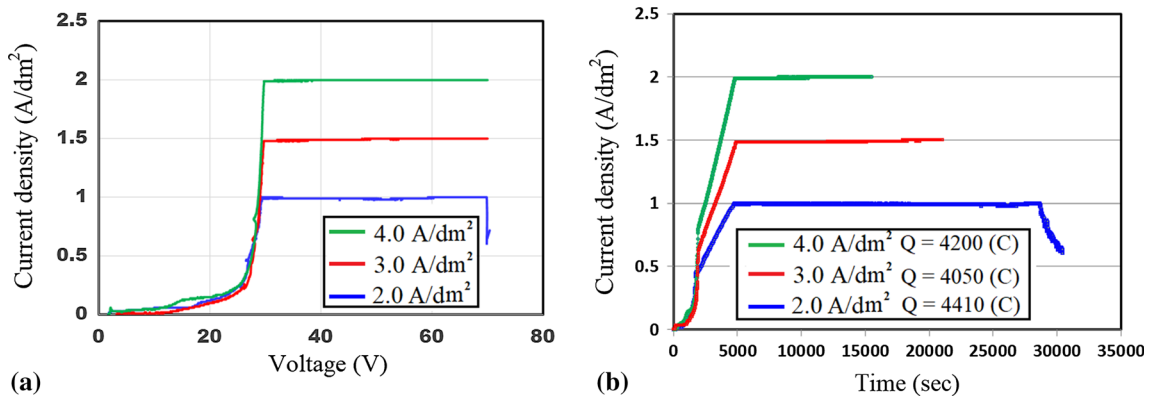


**Fig. 9** (a) I-V curves and (b) I-T curves for AA 6061 alloy after hard anodizing treatment at  $-4^{\circ}\text{C}$ , 70 V, and various current densities: 2.0, 3.0, and 4.0 A/dm<sup>2</sup>

**Table 4** Thickness and hardness of anodized aluminum oxide film obtained by anodization treatment of AA 6061 (50 cm<sup>2</sup>) at  $-4^{\circ}\text{C}$  and 70V for various times

Symbol	Treatment	Current, A	Current density, A dm <sup>-2</sup>	Power, C	Measured thickness, $\mu\text{m}$	Calculated thickness, $\mu\text{m}$	Anodization efficiency, %	Hardness, HV <sub>1.0</sub>
L-H1	Hard Anodization	1.0	2	4410	99	60	60	576 ± 28
L-H2	Hard Anodization	1.5	3	4050	90	54	59	503 ± 20
L-H3	Hard Anodization	2.0	4	4200	94	57	60	525 ± 23

hollow tubes shrank after the sealing treatment due to the volume expansion resulting from the above phase transformation. For example, the inner diameters of the tubes were reduced from 150 to 80 nm and 20 nm after sealing treatments at 100°C for 60 min and 80 min, respectively. Moreover, the EDS analysis and element mapping images showed Al (63.65 wt.%), Mg (1.18 wt.%), Si (0.32 wt.%), and O (34.85 wt.%) distributed uniformly within the nanotubes.

The corrosion property of the aluminum anodized oxide film was also evaluated in 3.5 wt.% NaCl. Figure 12 shows the electrochemical behaviors of 6061 AA with and without anodization treatment determined by Tafel polarization measurement and AC impedance test. It can be clearly seen that, compared with 6061 AA with anodization treatment, AA 6061 without the anodized aluminum oxide film had a larger corrosion current density (Fig. 12a),  $10^{-2.7}$  A/cm<sup>2</sup>, and smaller

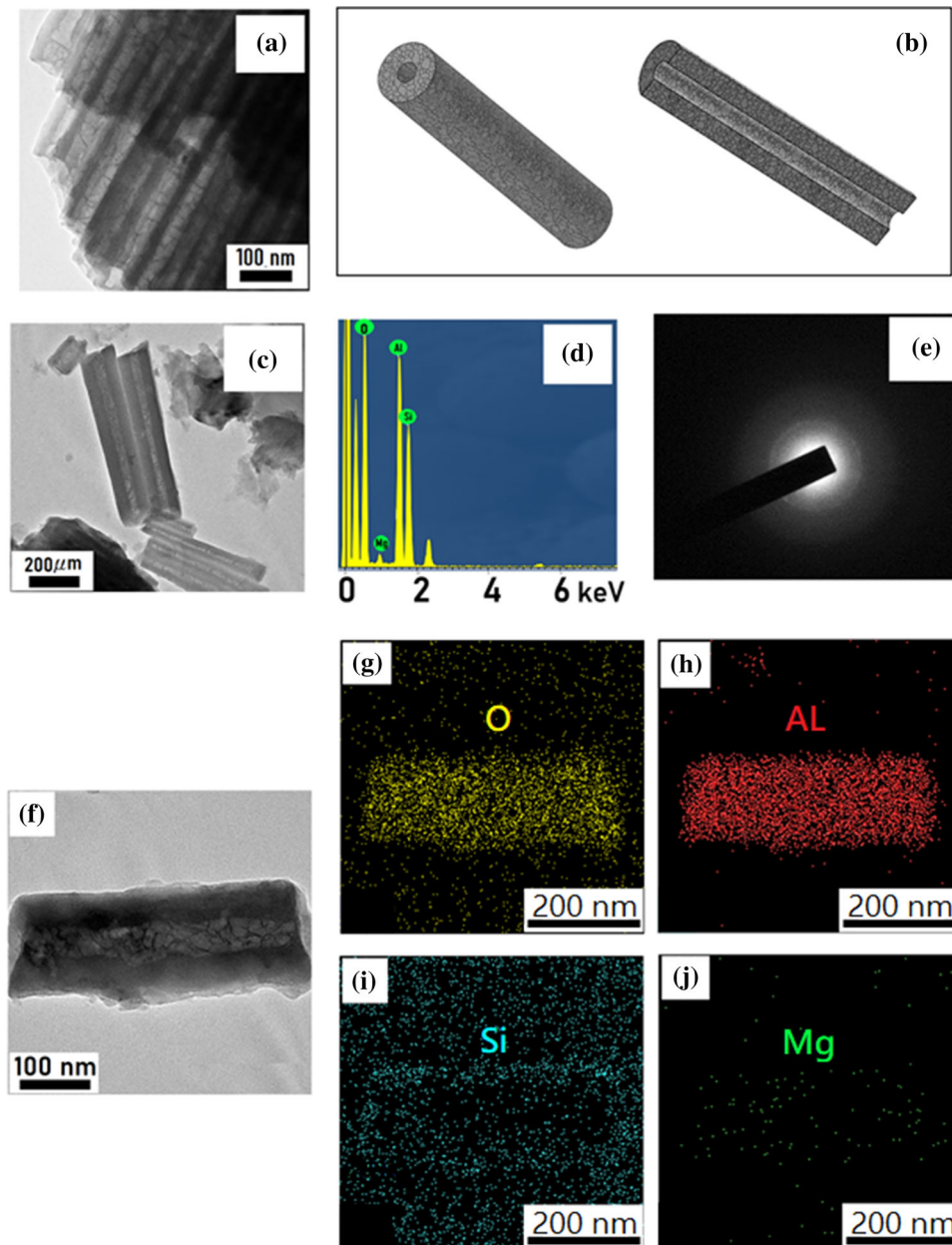


**Fig. 10** (a, c, f) TEM morphologies of aluminum oxide film revealing tube structure and some micro-cracks, (b) schematic diagrams illustrating the microstructural characterization of these aluminum oxide tubes, (d) EDS analysis, (e) diffraction pattern showing amorphous structure and (g-j) element mapping images

corrosion voltage,  $-0.56$  V (SCE), which indicates that the better corrosion resistance ability can be achieved by anodization treatment. On the other hand, from the AC impedance measurement (Fig. 12b), the Bode plots revealed that 6061 AA with the anodized oxide film had higher impedance ( $10^6$  ohm) than that of the bare 6061 AA ( $10^2$  ohm) in the lower frequency range. Furthermore, Nyquist plots also showed that the 6061

AA with anodization oxide film had higher impedance (Fig. 12c-d). Therefore, from the above results, it can be deduced that the better corrosion resistance resulted from the anodized oxide film with large resistivity. In addition, Sarah L'Haridon-Quaireau et al. also investigated the effects of parameters on pitting and uniform corrosion of the aluminum alloy 6061-T6 in the conditions found in material testing

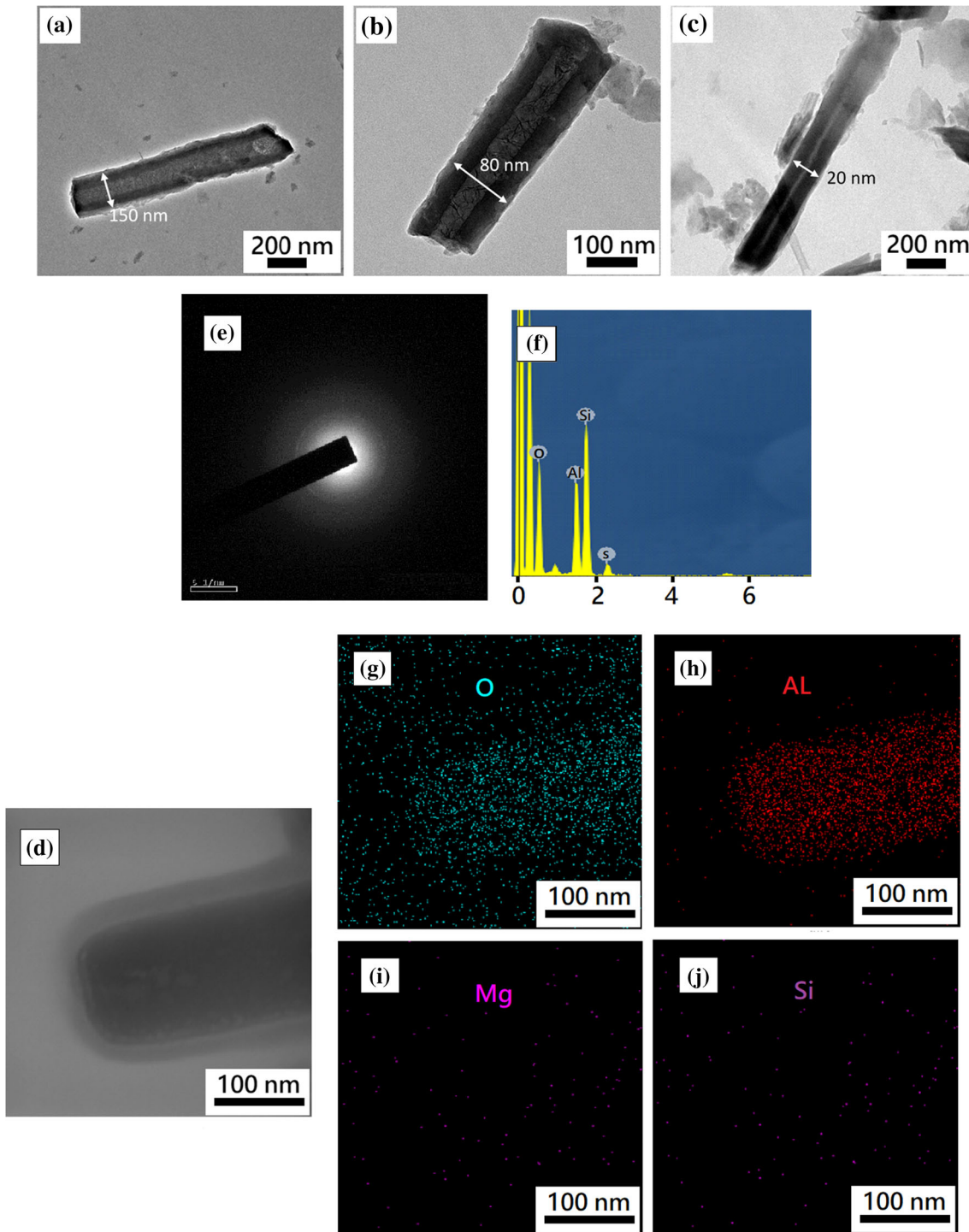


**Fig. 11** TEM morphologies showing the microstructural characterization of anodized aluminum oxide (a) before, (b, c, d) after sealing treatment at 100°C for (b, d) 60 min and (c) 80 min, (e) diffraction pattern. (f) EDS analysis, and (g-j) element mapping images

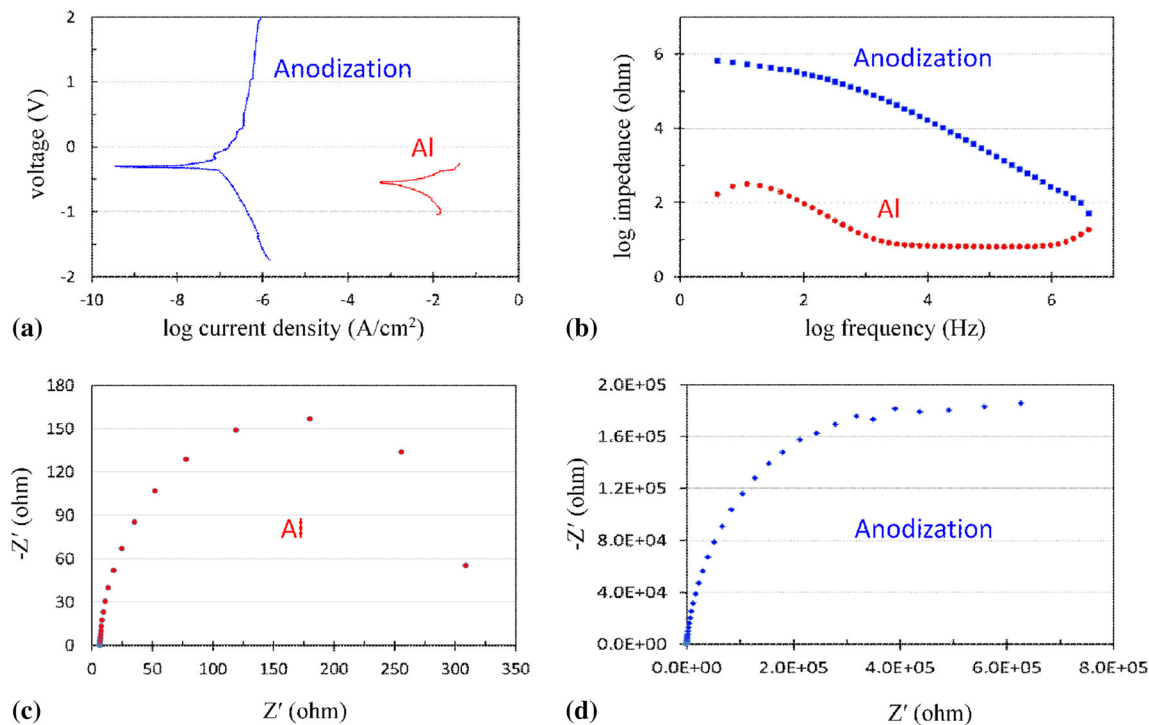


**Fig. 12** Electrochemical test curves of 6061 AA with and without anodization treatment. (a) Tafel curves, (b) Bode plots, and Nyquist plots of 6061 AA (c) with, and (d) without anodization treatment

reactors (MTR). They also found that at low temperature (70°C), the film is composed of two layers of different aluminum hydroxide phases. These two phases have different corrosion behaviors depending on the PH (45).

## 4. Conclusions

In the present study, an aluminum oxide layer was produced under different anodization treatment conditions, and oxide films with various properties, including thickness, hardness, and microstructure, were measured. The anodization process included pre-treatment by annealing, mechanical grinding, and chemical polishing; anodization; and post-treatment of acidification, dyeing, water sealing, polishing, laser engraving, electrophoresis, and curing. In the process, the pre-treatment by sandblasting gave the AA 6061 surface uniform roughness. Chemical polishing removed the slight friction scratches and contaminants on the AA 6061 surface, smoothed the surface, and produced a surface with a high mirror brightness.

Furthermore, the anodic oxide film has the following characteristics:

1. Anodic oxide film with hollow tube structures having inner diameters of 70-90 nm and outer diameters of 240-280 nm can be obtained with the mild anodization treatment. Furthermore, the oxide film can achieve higher hardness and resistance to corrosion through the sealing process, which can effectively decrease the size of the tubes due to the volume expansion effect (23%) during the sealing treatment. The hardness values of the films are between 142 and 359 HV<sub>1.0</sub>.

2. Anodic oxide films of different colors, namely, translucent (suitable for dyeing), brown (suitable for dyeing with dark colors), and black (unsuitable for dyeing), were obtained when the current densities of the anodization treatment (22°C) were from 1 to 4 A/dm<sup>2</sup>, 5 to 8 A/dm<sup>2</sup>, and 9 to 12 A/dm<sup>2</sup>, respectively.
3. Anodic oxide film with a higher hardness can be obtained at a lower anodization temperature (0°C) than at room temperature (22°C).
4. The sealing process can reduce the inner diameters of the anodic tubular film from 150 to 80 nm and 20 nm after sealing treatments at 100°C for 60 min and 80 min, respectively.
5. A two-step current density approach was used in the hard anodization treatment. The hardness values of the film were 576, 503, and 525 HV<sub>1.0</sub>, and the anodization efficiencies were 60, 59, and 60%, when the current densities were 2, 3, and 4 A/dm<sup>2</sup>, respectively.
6. 6061 AA after anodization presents very good corrosion resistance, according to the Tafel polarization measurement and AC impedance tests. The 6061 AA with anodic film has a higher corrosion voltage (-0.3 V, SCE), lower corrosion current density (10<sup>-7.8</sup> A/cm<sup>2</sup>), and higher impedance (10<sup>6</sup> ohm) than those of 6061 AA without anodization treatment (corrosion voltage, -0.56 V, SCE; corrosion current density, 10<sup>-2.7</sup> A/cm<sup>2</sup>; impedance, 10<sup>2</sup> ohm).

## Funding

This work was financially supported by the Ministry of Science and Technology, Taiwan under Contract No. MOST 109-2221-E-

## References

1. B. Stojanovic and I. Epler, Application of Aluminum and Aluminum Alloys in Engineering, *Appl. Eng. Lett.*, 2018, **3**(2), p 52–62.
2. H. Okuyucu, A. Kurt and E. Arcaklioglu, Artificial Neural Network Application to the Friction Stir Welding of Aluminum Plates, *Mater. Design*, 2007, **28**(1), p 78–84.
3. P. Blanchard, C. Colombie, V. Pellerin, S. Fayeulle and L. Vincent, Material Effects in Fretting Wear: Application to Iron, Titanium, and Aluminum Alloys, *Metall. Trans. A*, 1991, **22**, p 1535–1544.
4. D.G. Piercey and T.M. Klapoetke, Nanoscale Aluminum-Metal Oxide (Thermite) Reactions for Application in Energetic Materials, *Cent. Eur. J. Ener. Mater.*, 2010, **7**(2), p 115–129.
5. J.A. Puszynski, Reactivity of Nanosize Aluminum with Metal Oxides and Water Vapor, *Mat Res Soc Symp Proc*, 2004 <https://doi.org/10.1557/PROC-800-AA6.4>
6. J.R. Jouet, A.D. Warren, D.M. Rosenberg, V.J. Bellitto, K. Park and M.R. Zachariah, Surface Passivation of Bare Aluminum Nanoparticles Using Perfluoroalkyl Carboxylic Acids, *Chem. Mater.*, 2005, **17**, p 2987–2996.
7. M. Zuo, M. Sokoluk, C. Cao, J. Yuan, S. Zheng and X. Li, Microstructure Control and Performance Evolution of Aluminum Alloy 7075 by Nano-Treating, *Sci. Rep.*, 2019, **9**, p 1–11.
8. J.F. Peng et al., Study on the Damage Evolution of Torsional Fretting Fatigue in a 7075 Aluminum Alloy, *Wear*, 2018, **402–403**, p 160–168.
9. C.C. Chen, D. Fang and Z. Luo, Fabrication and Characterization of Highly-Ordered Valve-Metal Oxide Nanotubes and their Derivative Nanostructures, *Rev. Nanosci. Nanotechnol.*, 2012, **1**, p 229–256.
10. P.C. Chen, S.J. Hsieh, C.C. Chen and J. Zou, Fabrication and Characterization of Chemically Sensitive Needle Tips with Aluminum Oxide Nanopores for pH Indication, *Ceram. Int.*, 2013, **39**(3), p 2597–2600.
11. C. Alexander, G.L. Hager, Method of multi-coloring anodized aluminum. US patent, US 3099610A, 1963
12. C.E. Michelson, Process for coloring an anodized aluminum sheet. US patent, US 3218243A, 1965
13. S. Kia, H.H. Kuo, Y.M. Wang, Color Stabilization of Anodized Aluminum Alloys. US patent, US 20060260947A1, 2006
14. B. Platschek, A. Keilbach and T. Bein, Mesoporous Structures Confined in Anodic Alumina Membranes, *Adv. Mater.*, 2011, **23**(21), p 2395–2412.
15. T. Kumeria, M.D. Kurkuri, K.R. Diener, L. Parkinson and D. Losic, Label-Free Reflectometric Interference Microchip Biosensor Based on Nanoporous Alumina for Detection of Circulating Tumour Cells, *Biosens. Bioelectr.*, 2012, **35**(1), p 167–173.
16. M. Wang, G. Meng, Q. Huang, M. Li, Z. Li and C. Tang, Fluorescence Detection of Trace PCB101 Based on P1TC Immobilized on Porous AAO Membrane, *Analyst*, 2011, **136**(2), p 278–281.
17. G.J. Wang, Y.S. Chen, Nano-hemisphere structure array mold manufacturing method and its mold, R. O. C. patent, TW 201300309A, 2013
18. W. Shi, Y. Shen, D. Ge, M. Xue, H. Cao, S. Huang, J. Wang, G. Zhang and F. Zhang, Functionalized Anodic Aluminum Oxide (AAO) Membranes for Affinity Protein Separation, *J. Membr. Sci.*, 2008, **325**(2), p 801–808.
19. J. Fu, P. Mao and J. Han, Artificial Molecular Sieves and Filters: A New Paradigm for Biomolecule Separation, *Trends Biotechnol.*, 2008, **26**(6), p 311–320.
20. F. Matsumoto, K. Nishio and H. Masuda, Flow-Through-Type DNA Array Based On Ideally Ordered Anodic Porous Alumina substrate, *Adv. Mater.*, 2004, **16**(23–24), p 2105–2108.
21. E.E.L. Swan, K.C. Popat, C.A. Grimes and T.A. Desai, Fabrication and Evaluation of Nanoporous Alumina Membranes for Osteoblast Culture, *J. Biomed. Mater. Res. Part A*, 2005, **72**(3), p 288–295.
22. M. Vallet-Regi, I. Izquierdo-Barba and M. Colilla, Structure and Functionalization of Mesoporous Bioceramics for Bone Tissue Regeneration and Local Drug Delivery, *Philos. Trans. Royal Soc. A: Math., Phys. Eng. Sci.*, 2012, **370**(1963), p 1400–1421.
23. Y.S. Lin, S.L. Huang, Y.C. Tsai, Skin covering and preparation method thereof. R. O. C. patent, TW I565484, 2017
24. M. Manzano and M. Vallet-Regi, New developments in ordered mesoporous materials for drug delivery, *J. Mater. Chem.*, 2010, **20**(27), p 5593–5604.
25. C-C Chen, A metal tip with a large surface area. R. O. C. patent, TW 201905218A, 2019
26. C.Y. Chen, S.H. Chen, C.C. Chen and J.S. Lin, Using Positive Pressure to produce a Sub-micron Single-Crystal Column of Cesium Iodide (CsI) for Scintillator Formation, *Mater. Lett.*, 2015, **148**, p 138–141.
27. M. Nicholas, Jr W.A. Mitchell, Decorative aluminum surface. US patent, US 2941930A, 1960
28. W.J. Bernard, S.P. Szpak, Two-stage anodization of capacitor electrodes. US patent, US 4131520A, 1978
29. J.K. Khosla, US patent. Dual anodization surface treatment. US 8398841B2, 2013
30. S. Das and W. Yin, Trends in the Global Aluminum Fabrication Industry, *JOM*, 2007, **59**, p 83–87.
31. F. Czerwinski, Cerium in Aluminum Alloys, *J. Mater. Sci.*, 2020, **55**, p 24–72.
32. S. Alkahtani, E. Elgallad, M. Tash, A. Samuel and F. Samuel, Effect of Rare Earth Metals on the Microstructure of Al-Si Based Alloys, *Materials*, 2016, **9**(45), p 1–13.
33. S.K. Naik and R.R. Ghatak, Coal-Sourcing Options for Captive Power Plants of Aluminum Smelters in India Issues and Challenge, *Innov. Technol., Market Ecosyst.*, 2020 [https://doi.org/10.1007/978-3-030-23010-4\\_4](https://doi.org/10.1007/978-3-030-23010-4_4)
34. M. Mehdizade, M. Soltanieh and A.R. Eivani, Investigation of Anodizing Time and Pulse Voltage Modes on the Corrosion Behavior of Nanostructured Anodic Layer in Commercial Pure Aluminum, *Surface Coat. Technol.*, 2019, **358**, p 741–752.
35. Y. Gao, Xu. Xiaolei, Z. Yan and G. Xin, High Hardness Alumina Coatings Prepared by Low Power Plasma Spraying, *Surf. Coat. Technol.*, 2002, **154**, p 189–193.
36. A. Khakzad, S.M. Mousavi Khoi and S.A. Tayebifard, Alumina-Silica Composite Coatings on Aluminum by Plasma Electrolytic Oxidation: The Effect of Coating Time on Microstructure, Phase, and Corrosion Behavior, *J. Mater. Eng. Perform.*, 2017, **26**, p 2663–2670.
37. Z. Yang, R.Q. Wang, C. Liu, Y.K. Wu, D.D. Wang, X.T. Liu, X.Z. Zhang, G.R. Wu and D.J. Shen, The Electrochemical Corrosion Behavior of Plasma Electrolytic Oxidation Coatings Fabricated on Aluminum in Silicate Electrolyte, *J. Mater. Eng. Perform.*, 2019, **28**, p 3652–3660.
38. M. Mahmoudi, H. Maleki-Ghaleh, M. Kavanlouei and E. Aghaie, Effect of Al<sub>2</sub>O<sub>3</sub>-Ti Composite Coating on Corrosion Behavior of TiAl<sub>6</sub>V<sub>4</sub> Alloy, *Mater. Corros.*, 2015, **66**, p 479–485.
39. M. Mahmoudi, H. Maleki-Ghaleh and M. Kavanlouei, Electrophoretic Deposition and Reaction-Bond Sintering of Al<sub>2</sub>O<sub>3</sub>/Ti Composite Coating: Evaluation of Microstructure, Phase and Wear Resistance, *Bull. Mater. Sci.*, 2015, **38**(2), p 351–356.
40. M.A. Fauzi, M.B. Uday, H. Zuhailawati and A.B. Ismail, Microstructure and Mechanical Properties of Alumina-6061 Aluminum Alloy Joined by Friction Welding, *Mater. Design*, 2010, **31**(2), p 670–676.
41. C.A. Biffi, J. Fiocchi and A. Tuissi, Selective Laser Melting of AlSi10Mg: Influence of Process Parameters on Mg<sub>2</sub>Si Precipitation and Si Spheroidization, *J. Alloys Compd.*, 2018, **755**, p 100–107.
42. S.H. Lee, Y. Saito, T. Sakai and H. Utsunomiya, Microstructures and Mechanical Properties of 6061 Aluminum Alloy Processed by Accumulative Roll-Bonding, *Mater. Sci. Eng.: A*, 2002, **325**(1–2), p 228–235.
43. M. Pourbaix, *Atlas of Electrochemical Equilibria in Aqueous Solution*, NACE, USA, 1974, p 213
44. R.K. Choudhary, K.P. Sreeshma and P. Mishra, Effect of Surface Roughness of an Electropolished Aluminum Substrate on the Thickness, Morphology, and Hardness of Aluminum Oxide Coatings Formed During Anodization In Oxalic Acid, *J. Mater. Eng. Perform.*, 2017, **26**, p 3614–3620.
45. S. L'Haridon-Quaireau, M. Laot, K. Colas, B. Kapusta, S. Delpech and D. Gosset, Effects of Temperature and pH on Uniform and Pitting Corrosion of Aluminium Alloy 6061–T6 and Characterisation of the Hydroxide Layers, *J. Alloys Compd.*, 2020, **833**, p 155146.

**Publisher's Note** Springer Nature remains neutral with regard to jurisdictional claims in published maps and institutional affiliations.